Progress In Electromagnetics Research M, Vol. 34, 107–116, 2014

Analysis of Scattering from Dielectric Rough Surfaces by Hybrid FEM/BIE

Runwen Xu*, Lixin Guo, and Xiao Meng

Abstract—To study electromagnetic scattering from dielectric rough surfaces, a hybrid finite element method (FEM) combined with boundary integral equations (BIE) is extended to the scattering problem with two half-open regions. Integral boundaries, as truncated boundaries of the FEM region, are employed as artificial boundaries of dielectric rough surfaces above and below the rough surface. In the hybrid method, conformal integral boundaries are introduced to reduce the computational region. The validity of our hybrid method is examined by available solutions got from the method of moment (MoM), which indicates the feasibility of our scheme in simulating the scattering from dielectric rough surfaces. Bistatic scattering coefficient from dielectric rough surfaces is studied in this paper for both polarizations, and functional dependence upon different parameters are numerically discussed.

1. INTRODUCTION

The scattering from random rough surfaces has been a topic of continuing interest for many years due to its broad applications, such as remote sensing, target detection, material science, oceanography, academic applications, etc. Some numerical methods have been developed, such as the method of moment (MoM) [1], the forward backward method (FBM) [2], the finite element method (FEM) [3], and others in the frequency domain, while time domain integral equation (TDIE) [4] and finite difference time domain method (FDTD) [5] are widely used in the time domain. The boundary integral methods can take the Sommerfeld radiation condition into account by the adoption of a proper Green function, and these methods can be seen as the most precise numerical methods. However, boundary integral methods are hardly applied to electromagnetic problems consisting of inhomogeneous complex structures. On the other hand, the finite element method is one of the most appealing numerical methods for the analysis of electromagnetic problems, especially for complex dielectric structures. In an unbounded computational region, approximate absorbing boundaries are always applied for truncated boundaries, and most works are focused on targets of a limited size or conducting rough surfaces, such as absorbing boundary condition (ABC) [6] and perfectly matched layer (PML) [7]. Liu and Jin introduced FEM/PML in [8] to discuss the scattering from a rough surface, and they studied bistatic scattering from a target at the low altitude above a conducting rough sea surface. Monte Carlo-based characteristic basis finite element method (MC-CBFEM) [9] is employed by Ozgun to study the scattering from an object on/above a rough sea surface assumed that the rough sea is approximated as a conducting medium. However, these approximation absorbing boundaries often need to be set far enough away from the model surface or only limited to some particular problems, which leads to unexpected precision.

To overcome shortcomings of the traditional FEM and the boundary integral method, a hybrid FEM/BIE method is introduced to keep the advantages of two numerical methods. A hybrid method based on the volume-surface integral equation (VSIE) and the impedance matrix interpolation technique is presented in [10] for the fast analysis of microstrip antennas in frequency sweeps. Alavikia and Ramahi applied a hybrid finite element method combined with the surface integral equation method [11] to study

Received 22 November 2013, Accepted 20 December 2013, Scheduled 25 December 2013

* Corresponding author: Runwen Xu (rwxu719@126.com).

The authors are with the School of Physics and Optoelectronic Engineering, Xidian University, Xi'an 710071, China.

electromagnetic scattering from cylindrical objects above a conductive plane surface. A finite element-boundary integral-domain decomposition method is presented in [12] for analyzing electromagnetic scattering problems involving multiple cavities. Hybrid FEM/BIE is presented by Li et al. in [13] to study electromagnetic scattering from a perfectly electric conducting (PEC) rough surface. The hybrid finite-element/boundary-integral method (FEBI) combined with the multilevel fast multipole algorithm (MLFMA) has been applied in [14] to model scattering problems of inhomogeneous media. The hybrid FEM/BIE can not only deal with scattering problems of dielectric models easier than MoM, but also reduce the computation region and maintain higher precision compared with applications of approximate absorbing boundaries. Although the studies on scattering problems of rough surfaces have been developed for decades, numerical simulations with FEM for dielectric rough surfaces still need to be made a further study.

Compared with published papers, a hybrid FEM/BIE is extended into the scattering problem of dielectric rough surfaces, and conformal integral boundaries are developed. Unlike the PEC rough surface, the space is divided into two domains by dielectric rough surface. In the past, the rough surface are usually assumed as a PEC model [8, 9] when FEM is applied to simulate the scattering problem. Based on [13], FEM/BIE is extended into the scattering from the dielectric model. In the hybrid method, conformal integral boundaries are applied in the space to truncate the infinite computational region of a rough surface, while FEM is used to simulate the electromagnetic scattering problem in the interior region. To couple scattering systems between the interior region and the exterior region, continuity conditions are applied on integral boundaries. The validity of this hybrid method is examined by available solutions of MoM.

2. FORMULATIONS AND EQUATIONS

The two-dimensional model of our interest is depicted in Figure 1, and theoretical formulas of scattering from dielectric rough surfaces are deduced in this section. The incident wave impinges on one-dimensional dielectric rough surface with an incidence angle θ_{inc} and an scattering angle θ_{scat} defined as in Figure 1. For the problem with two half-open computational regions, artificial boundaries should be not only built above rough surfaces, but also set below rough surfaces in the implementation of FEM. Artificial boundaries Γ_{UBIE} and Γ_{DBIE} split computational domain into the upper region Ω_{up}, interior region Ω_{in}, and the region below a rough surface Ω_{down}. Unlike truncated boundaries of PML, the shape of artificial integral boundaries in FEM/BIE is arbitrary which has a little influence on calculational results, and can be set even on the surface of a model. To reduce the computational region as possible as we can, an integral boundary Γ_{UBIE} in the upper space Ω_{up} is set on the profile of a rough surface, and an artificial boundary Γ_{DBIE} is built at a height of 0.1λ with a conformal profile below the rough surface to enclose the whole model.

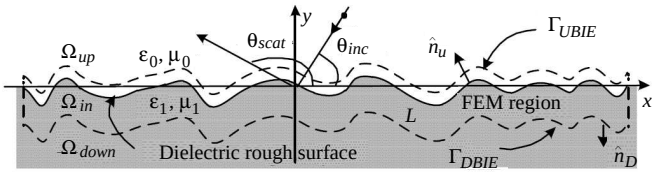

Figure 1. Geometry of scattering from a dielectric rough surface.

For each realization of the Monte Carlo method, one-dimensional random rough surface can be generated by a corresponding power spectrum. In this paper, Gaussian rough surfaces are chosen to study, whose power spectrum function can be written as follows

$$S(k_i) = \frac{\delta^2 l}{2\sqrt{\pi}} \exp\left(-k_i^2 l^2/4\right) \tag{1}$$

where δ denotes the root mean square height (rms), and l represents the correlation length (l_c).

Rough surfaces should be truncated into a finite computational domain in our discussion, which can introduce artificial reflection. To reduce computational error caused by the truncation effect, an

incident wave used here is taper incident wave, which is proposed by Thorsos [15], and can be expressed as

$$\Phi^{inc} = \exp\ [-j\mathbf{k}\cdot\mathbf{r}(1+w(\mathbf{r}))]\cdot\exp\left[-(x-y\cdot\cot\theta_{inc})^2/g^2\right] \tag{2}$$

where $\mathbf{k}$ denotes the wave number, g the tapered factor of an incident wave, $\mathbf{r}$ a position vector of the observation point in the space, and

$$w(\mathbf{r}) = \exp\left[2\left(x-y\cdot\cot\theta_{inc}\right)^2/g^2-1\right]/(kg\cdot\sin\theta_{inc})^2 \tag{3}$$

For both transverse electric (TE) polarization (where the electric field has a component only along axis z) and transverse magnetic (TM) polarization (where the magnetic field has a component only along axis z), total fields in the space are governed by the Helmholtz equation

$$\left[\frac{\partial}{\partial x}\left(\frac{1}{\rho}\frac{\partial}{\partial x}\right)+\frac{\partial}{\partial y}\left(\frac{1}{\rho}\frac{\partial}{\partial y}\right)+\beta\right]\Phi(\mathbf{r}) = f(\mathbf{r}) \tag{4}$$

in which $\Phi(\mathbf{r})$ denotes the total field. For TE case

$$\left.\begin{aligned}&\rho=\mu_r\\&\beta=k_0^2\varepsilon_r\\&f(\mathbf{r})=jk_0Z_0J_z(\mathbf{r})\end{aligned}\right\} \tag{5}$$

For the TM case

$$\left.\begin{aligned}&\rho=\varepsilon_r\\&\beta=k_0^2\mu_r\\&f(\mathbf{r})=-\frac{1}{\rho}\left[\nabla\times\mathbf{J}(\mathbf{r})\right]_z\end{aligned}\right\} \tag{6}$$

where $[\nabla\times\mathbf{J}(\mathbf{r})]_z = [\nabla\times\mathbf{J}(\mathbf{r})]\cdot\hat{z}$; k_0 is the wavenumber of the free space; Z_0 denotes the characteristic impedance; $\mathbf{J}(\mathbf{r})$ represents the current density existing in the space, and it induces the tapered incident wave; $\varepsilon_r = \varepsilon_r' - j\varepsilon_r''$ is the permittivity; μ_r is the permeability of the computational space.

On artificial surfaces Γ_{UBIE} and Γ_{DBIE}, boundary conditions can be assumed as follows for simplification:

$$\left.\frac{1}{\rho}\frac{\partial\Phi}{\partial n}\right|_{\Gamma_{UBIE}\text{ or }\Gamma_{DBIE}} = -\psi \tag{7}$$

where $\partial/\partial n$ is the corresponding normal derivative of Γ_{UBIE} or Γ_{DBIE}. Based on the published work, the scattering problem in the interior domain Ω_{in} can be solved by the functional analysis [16], whose equivalent variational problem can be given by

$$\delta F(\Phi) = 0 \tag{8}$$

where

$$F(\Phi)=\frac{1}{2}\iint_{\Omega_{in}}\left[\frac{1}{\rho}\left(\frac{\partial\Phi}{\partial x}\right)^2+\frac{1}{\rho}\left(\frac{\partial\Phi}{\partial y}\right)^2-k_0^2\upsilon\Phi^2\right]d\Omega-\iint_{\Omega_{in}}f\Phi d\Omega+\int_{\Gamma_{UBIE}}\Phi\psi_U d\Gamma+\int_{\Gamma_{DBIE}}\Phi\psi_D d\Gamma \tag{9}$$

In the above functional equation, for TE case, $\rho=\mu_r$, $\upsilon=\varepsilon_r$; for TM case, $\rho=\varepsilon_r$, $\upsilon=\mu_r$. In the finite domain Ω_{in}, the part $\iint_{\Omega_{in}} f\Phi d\Omega$ can be removed because there is no current in this region.

In order to obtain integral equations of $\Phi(r)$ in regions Ω_{up} and Ω_{down}, the Green's function in the space $G(r,r')$ needs to be introduced, which can be written as

$$G(r,r') = \frac{1}{4j}H_0^2\left(k\left|\mathbf{r}-\mathbf{r}'\right|\right) \tag{10}$$

where $k = k_0\sqrt{\varepsilon_r\mu_r}$ is the wavenumber of the computational space. The Sommerfeld radiation boundary condition is satisfied automatically above or below a rough surface, and the following differential equation can also be satisfied above or below the rough surface

$$\nabla^2G(\mathbf{r},\mathbf{r}')+k^2G(\mathbf{r},\mathbf{r}') = -\delta(\mathbf{r}-\mathbf{r}') \quad \mathbf{r}'\in\Omega_\infty \tag{11}$$

In the region above the rough surface, there is an incidence source existing in the space. Combining Eqs. (4), (11) with the Green's scalar theorem, we have

$$\Phi(\mathbf{r}') = \int_{\Gamma_{Rs}} \left[\Phi(\mathbf{r})\frac{\partial G_U(\mathbf{r},\mathbf{r}')}{\partial n_U} - G_U(\mathbf{r},\mathbf{r}')\frac{\partial \Phi(\mathbf{r})}{\partial n_U}\right] d\Gamma + \int_{\Gamma_\infty} \left[\Phi(\mathbf{r})\frac{\partial G_U(\mathbf{r},\mathbf{r}')}{\partial n_U} - G_U(\mathbf{r},\mathbf{r}')\frac{\partial \Phi(\mathbf{r})}{\partial n_U}\right] d\Gamma - \iint_{\Omega_{up}} \left[G_U(\mathbf{r},\mathbf{r}')f(\mathbf{r})\right] d\Omega \tag{12}$$

where Γ_{Rs} is the truncated domain of a rough surface; Γ_∞ includes the infinite boundary above a rough surface, the right part of a rough surface which overflows from the truncated domain Γ_{Rs}, and the left part of a rough surface which overflows from the truncated domain Γ_{Rs}. On the infinite boundary above the rough surface of Γ_∞, both $\Phi(\mathbf{r})$ and $G_U(\mathbf{r},\mathbf{r}')$ satisfy the Sommerfeld radiation conditions, and the incident fields on the parts of the rough surface which overflow from the truncated domain Γ_{Rs} are almost zero due to the adoption of the tapered incident wave. So the right second boundary integral can be removed. When $\mathbf{r}'$ approach Γ_{UBIE} infinitely in the domain Ω_{up}, the boundary integral equation on Γ_{UBIE} can be obtained

$$\Phi^{inc}\left(\mathbf{r}'\right) = \Phi\left(\mathbf{r}'\right) - \int_{\Gamma_{UBIE}} \left[\Phi(\mathbf{r})\frac{\partial G_U(\mathbf{r},\mathbf{r}')}{\partial n_U} - G_U(\mathbf{r},\mathbf{r}')\frac{\partial}{\partial n_U}\Phi(\mathbf{r})\right] d\Gamma \tag{13}$$

where $\Phi^{inc}(\mathbf{r}') = -\iint_{\Omega_{up}} [G_U(\mathbf{r},\mathbf{r}')f(\mathbf{r})]d\Omega$ denotes the incident tapered wave induced by the current in the space.

As formula deductions in the region Ω_{up}, the total field $\Phi(\mathbf{r})$ and the Green's function $G_D(\mathbf{r},\mathbf{r}')$ in the region Ω_{down} can also satisfy Eqs. (4) and (11), respectively. Unlike in the region Ω_{up}, there is no source in the region Ω_{down}, so the part about the source $f(\mathbf{r})$ in Eq. (4) can be removed. The integral equation on the boundary Γ_{DBIE} can be written as

$$0 = \Phi\left(\mathbf{r}'\right) - \int_{\Gamma_{DBIE}} \left[\Phi(\mathbf{r})\frac{\partial G_D(\mathbf{r},\mathbf{r}')}{\partial n_D} - G_D(\mathbf{r},\mathbf{r}')\frac{\partial}{\partial n_D}\Phi(\mathbf{r})\right] d\Gamma \tag{14}$$

Integral equations Eqs. (13) and (14) provide relationships between the electromagnetic field Φ and their normal derivative $\partial\Phi(\mathbf{r})/\partial n$ on integral boundaries Γ_{UBIE} and Γ_{DBIE}.

To couple the FEM and BIE systems, continuous conditions are applied on artificial boundaries Γ_{UBIE} and Γ_{DBIE}, which can be written as

$$\Phi|_{\Gamma_+} = \Phi|_{\Gamma_-} \tag{15}$$

$$\frac{1}{\rho_+}\frac{\partial \Phi}{\partial n}\bigg|_{\Gamma_+} = \frac{1}{\rho_-}\frac{\partial \Phi}{\partial n}\bigg|_{\Gamma_-} \tag{16}$$

where $\partial/\partial n$ is a corresponding normal derivative of Γ_{UBIE} or Γ_{DBIE}, and Γ_+ expresses the observation point approaching the integral boundary of Γ_{UBIE} or Γ_{DBIE} from the exterior region, while Γ_- denotes the observation point approaching the integral boundary of Γ_{UBIE} or Γ_{DBIE} from the interior region. For TE case, $\rho = \mu_r$, $\upsilon = \varepsilon_r$, and for TM case, $\rho = \varepsilon_r$, $\upsilon = \mu_r$. The total field and its normal derivative between the FEM region and the exterior region can be contacted by Eqs. (15) and (16).

Choosing linear interpolating functions as in [16] to discretize unknowns, unknowns in Eqs. (8), (13) and (14) can be written as

$$\Phi^e\left(\mathbf{r}\right) = \sum_{i=1}^{3} N_i^e \Phi_i^e \tag{17}$$

$$\Phi^s\left(\mathbf{r}\right) = \sum_{i=1}^{2} N_i^s \Phi_i^s \tag{18}$$

$$\psi^s\left(\mathbf{r}\right) = \sum_{i=1}^{2} N_i^s \psi_i^s \tag{19}$$

where Φ denotes the electromagnetic field and ψ the normal derivative $\partial\Phi(\mathbf{r})/\partial n$. The superscript e denotes the surface element and s the boundary element. Substituting Eqs. (17)–(19) into Eqs. (8), (13) and (14), coupled systems can be expanded to a weak form as the following linear matrix equation

$$\begin{bmatrix} \mathbf{K_{II}} & \mathbf{K_{IU}} & \mathbf{K_{ID}} \\ \mathbf{K_{UI}} & \mathbf{K_{UU}} & \mathbf{0} \\ \mathbf{K_{DI}} & \mathbf{0} & \mathbf{K_{DD}} \end{bmatrix} \begin{Bmatrix} \boldsymbol{\Phi}_\mathbf{I} \\ \boldsymbol{\psi}_\mathbf{U} \\ \boldsymbol{\psi}_\mathbf{D} \end{Bmatrix} = \begin{Bmatrix} \mathbf{0} \\ \mathbf{b_U} \\ \mathbf{0} \end{Bmatrix} \tag{20}$$

In the coupled system Eq. (20), element matrices of $\mathbf{K_{II}}$, $\mathbf{K_{IU}}$, $\mathbf{K_{ID}}$, $\mathbf{K_{UI}}$, $\mathbf{K_{UU}}$, $\mathbf{K_{DI}}$, $\mathbf{K_{DD}}$ and $\mathbf{b_U}$ are given as

$$[\mathbf{K_{II}}] = \iint_{\Omega_{in}^e} \left[\frac{1}{\rho} \left\{ \frac{\partial N^e}{\partial x} \right\} \left\{ \frac{\partial N^e}{\partial x} \right\}^T + \frac{1}{\rho} \left\{ \frac{\partial N^e}{\partial y} \right\} \left\{ \frac{\partial N^e}{\partial y} \right\}^T - k_0^2 \upsilon \left\{ N^e \right\} \left\{ N^e \right\}^T \right] dxdy \tag{21}$$

$$[\mathbf{K_{IU}}] = \int_{\Gamma_{UBIE}} \left\{ N^e \right\} \left\{ N_j^e \right\}^T d\Gamma \tag{22}$$

$$[\mathbf{K_{ID}}] = \int_{\Gamma_{DBIE}} \left\{ N^e \right\} \left\{ N_j^e \right\}^T d\Gamma \tag{23}$$

$$[\mathbf{K_{UI}}] = [\mathbf{K_{IU}}]^T - \int_{\Gamma_{UBIE}^s} \left[\left\{ N^s \right\} \int_{\Gamma_{UBIE}^t} \left\{ N^t \right\}^T \frac{\partial G_U}{\partial n'_U} d\Gamma' \right] d\Gamma \tag{24}$$

$$[\mathbf{K_{UU}}] = - \int_{\Gamma_{UBIE}^s} \left[\left\{ N^s \right\} \int_{\Gamma_{UBIE}^t} \left\{ N^t \right\}^T G_U d\Gamma' \right] d\Gamma \tag{25}$$

$$[\mathbf{K_{DI}}] = [\mathbf{K_{ID}}]^T - \int_{\Gamma_{DBIE}^s} \left[\left\{ N^s \right\} \int_{\Gamma_{DBIE}^t} \left\{ N^t \right\}^T \frac{\partial G_D}{\partial n'_D} d\Gamma' \right] d\Gamma \tag{26}$$

$$[\mathbf{K_{DD}}] = - \int_{\Gamma_{DBIE}^s} \left[\left\{ N^s \right\} \int_{\Gamma_{DBIE}^t} \left\{ N^t \right\}^T G_D d\Gamma' \right] d\Gamma \tag{27}$$

$$\{\mathbf{b_U}\} = \int_{\Gamma_{UBIE}^s} \left\{ N^s \right\} \Phi^{inc} d\Gamma \tag{28}$$

where $\boldsymbol{\Phi}$ denotes the matrix element of the electromagnetic field on nodes and $\boldsymbol{\psi}$ the matrix element about the normal derivative of the field on nodes. I denotes nodes of surface elements in the region Ω_{in} including nodes on Γ_{UBIE} and Γ_{DBIE}, U the nodal points on the integral boundary Γ_{UBIE}, D the unknowns on the artificial boundary Γ_{DBIE}, e the surface element, and s and t express the boundary elements. By using a direct linear system solver, values of the total field and its derivative on every point can be calculated, and then the bistatic scattering coefficient (BSC) for a tapered wave incidence can be calculated by the following equation

$$\mathrm{BSC} = \lim_{r \to \infty} 2\pi r \frac{\left| \Phi^{scat} \right|^2}{P_{inc}} \tag{29}$$

where

$$P_{inc} = \sqrt{\frac{\pi}{2}} g \sin\theta_{inc} \left(1 - \frac{1 + 2\cot^2\theta_{inc}}{2\left(k_0 g \cdot \sin\theta_{inc}\right)^2} \right) \tag{30}$$

3. PROCEDURE AND CODE VALIDATIONS

In this section, the bistatic scattering from dielectric rough surfaces under TE and TM cases are studied. Due to the randomness of rough surfaces, 30 samples of rough surfaces are chosen to average their electromagnetic fields to get a stable result. The edge size of discrete elements is about 0.05λ, the length of a rough surface L 25.6λ, the taper factor $g = L/4$, and the other parameters such as the incident angle θ_{inc}, the permittivity ε_r of rough surfaces, the root mean square height rms, and the

correlation length l_c are all given in the following figures. Combined with the sparse matrix algorithms, the complex sparse system of linear equations can be solved by Gaussian elimination.

To explore the validation of our FEM/BIE theory, the FEM/BIE codes are firstly examined by available solutions of MoM. Figure 2 gives comparative results of BSC with those of MoM in (a) and (b). Table 1 shows the comparisons of time and the number of nodes between two methods.

As shown in Figure 2, it is obvious that two different methods are in good agreement with each other for TE and TM cases, which not only assures the validation of our scheme, but also indicates the feasibility of our scheme in solving a scattering problem of dielectric rough surfaces. The differences between FEM/BIE and MoM are largely caused by the choice of grid size, the basic functions, as well as approximations in our programming. Due to FEM/BIE based on differential equations, increasing the mesh density or using higher order basis functions can lead to improving the accuracy of FEM/BIE.

To make a further verification on hybrid FEM/BIE, Figure 3 and Table 2 give other comparative

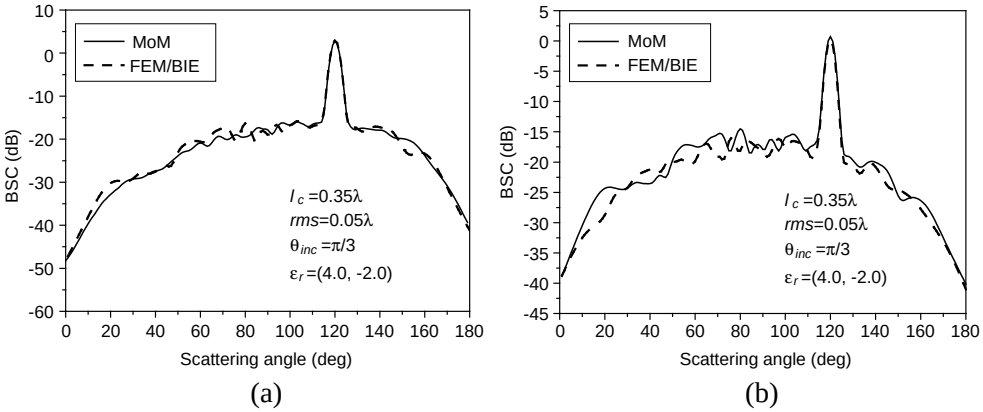

Figure 2. BSC from dielectric Gaussian rough surfaces: (a) TE case, (b) TM case.

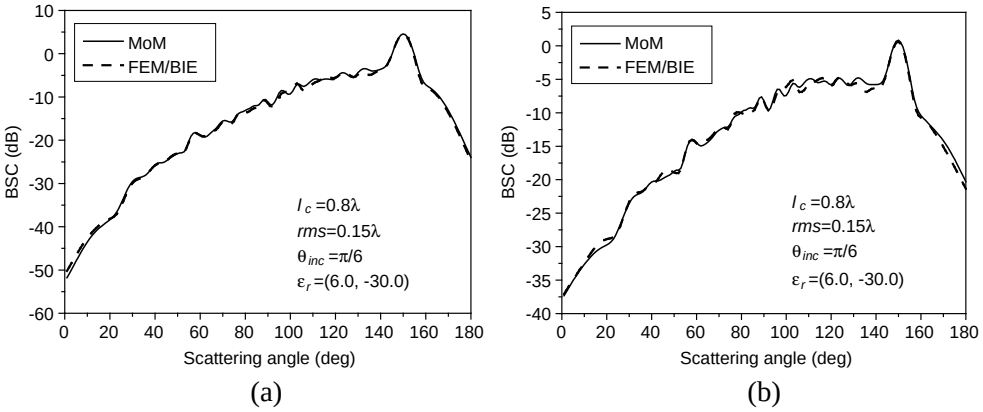

Figure 3. BSC from dielectric Gaussian rough surfaces: (a) TE case, (b) TM case.

Table 1. Comparison of time and the number of nodes between two different method (one sample).

Polarization	Method	Time (s)	Number of nodes
TM	MoM	4.63	512
	FEM/BIE	14.49	1052
TE	MoM	4.77	512
	FEM/BIE	35.47	1052

Table 2. Comparison of time and the number of nodes between two different method (one sample).

Polarization	Method	Time (s)	Number of nodes
TM	MoM	3.34	518
	FEM/BIE	4.76	1054
TE	MoM	3.37	518
	FEM/BIE	34.51	1054

results between FEM/BIE and MoM. Parameters of our model in Figure 2 are changed in this simulation to make a comparison, and the rough surface in this simulation has a larger rms value than that of Figure 2. In Figure 3, the well-matched results for both TE and TM cases in two simulations guarantee the feasibility of FEM/BIE again.

The hybrid method is versatile for different parameters of the rough surface. The shape of the artificial boundaries changes with the profile of the rough surface, and this measure can reduce the computational domain. Unlike traditional FEM based on PML or ABC, the shape of artificial boundaries have a little influence on results and can be set even on the surface of a model. Although this method can obtain an exact result, the number of unknowns and consumed time of hybrid FEM/BIE are more than those of MoM in above two simulations, because a mass of unavoidable meshes are created not only on its boundaries but also in the FEM domain in the simulation of FEM/BIE, whereas for MoM only the boundary of the rough surface need to be discretized. However, the memory consumed in simulations is less than that of traditional FEM based on ABC or PML, because our boundary is set only one layer of meshes far from the model surface. Although requiring more computer resource and time compared with MoM, hybrid FEM/BIE is a more appealing numerical method to deal with complex problems with an inhomogeneous medium because the problems about an inhomogeneous medium are hardly solved by the classical MoM, such as multilayer structures, inhomogeneous objects, and some buried targets exist below a ground.

4. RESULTS AND DISCUSSIONS

In the following, scattering characteristics of dielectric rough surfaces are mainly discussed by our hybrid method. Results of BSC with different incident angles are plotted in Figure 4 under TE case and TM case. It is found that peak values which correspond to main coherent components appear near specular angles for both TE case and TM case. With the decrease of incident angle θ_{inc}, the width of the specular peak broadens, and the peak value for TE case slightly increases, while the peak value for TM case decreases in the specular direction.

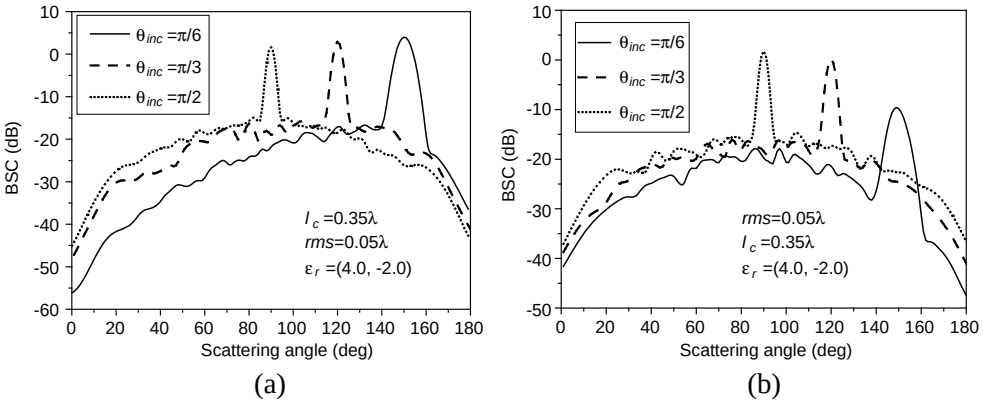

Figure 4. BSC of dielectric rough surfaces with different θ_{inc}: (a) TE case, (b) TM case.

Figure 5 illustrates results of BSC from dielectric Gaussian rough surfaces for different rms under TE case and TM case. With rms increasing, it is easily observed that incoherent components of the scattering field become larger in non-specular directions for both TE and TM cases. As rms is related to the degree of the roughness, rough surfaces become rougher with increasing rms, which can lead to an increase of the diffuse reflection and the reflection of energy in the non-specular directions.

Electromagnetic scattering from dielectric random rough surfaces with different correlation lengths l_c is examined in Figure 6. In numerical simulations, it can be concluded from the comparisons in Figures 6(a) and (b) that the curves are higher near the specular direction and lower in other directions with the correlation length increasing for TE and TM cases. Whens rms keeps constant, the ground roughness increases with the correlation length decreasing. As a result, the root mean square slope of

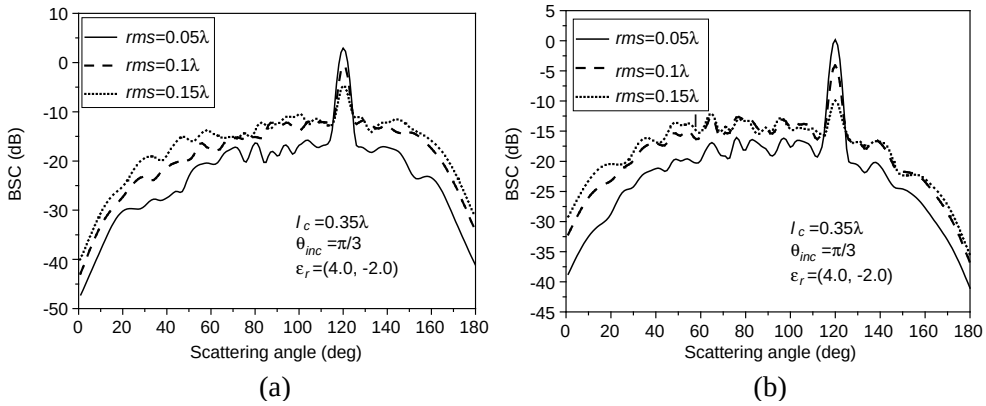

Figure 5. BSC of dielectric rough surfaces of different rms: (a) TE case, (b) TM case.

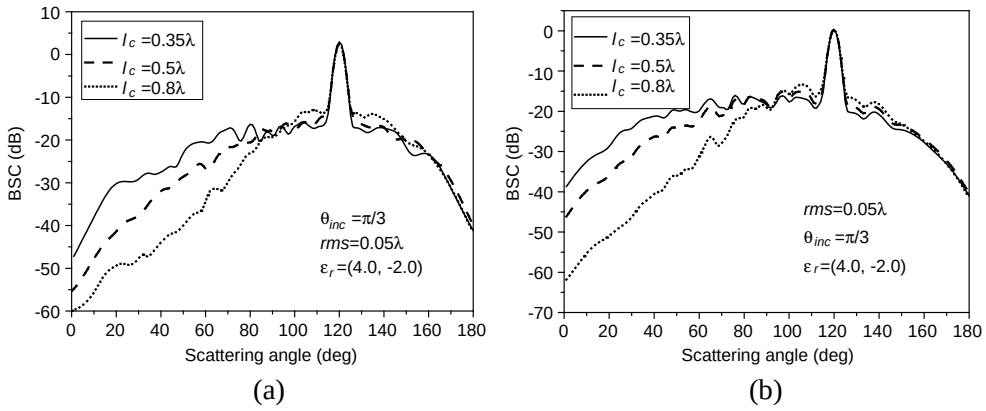

Figure 6. BSC of rough surfaces with different correlation lengths l_c: (a) TE case, (b) TM case.

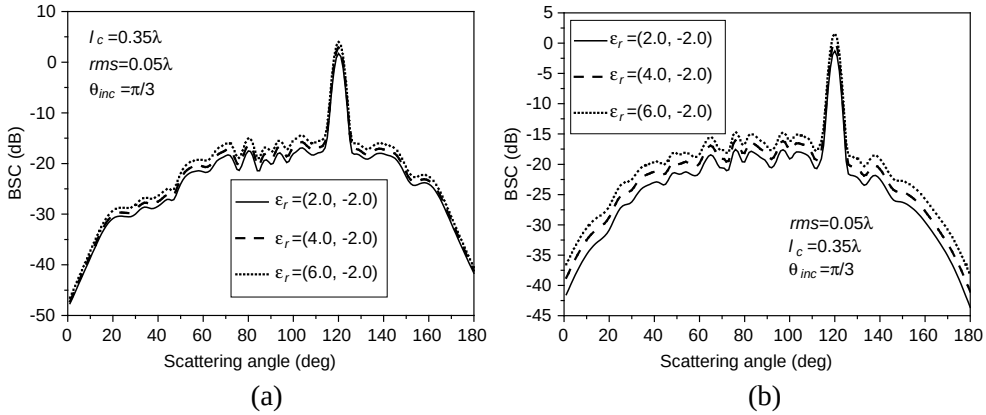

Figure 7. BSC of dielectric rough surfaces with different ε_r': (a) TE case, (b) TM case.

the rough surface will increase. Consequently, the scattered energy is more widely distributed in all directions due to the increase of the diffuse reflection when the root mean square slope becomes larger.

Bistatic scattering depending on different real parts of the permittivity ε_r' of dielectric rough surfaces is plotted in Figures 7(a) and (b) for different polarizations. From numerical results in Figure 7, it can be seen that BSC becomes large with the increase of ε_r' for TE and TM cases. This phenomenon can be explained by the theory of reflected coefficient, and the reflected coefficient has a rise when ε_r' increases.

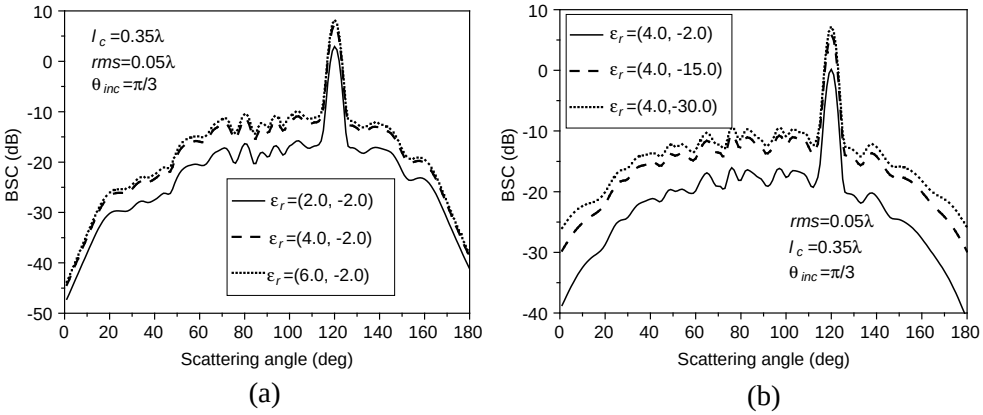

Figure 8. BSC of dielectric rough surfaces with different ε_r'': (a) TE case, (b) TM case.

Finally, electromagnetic scattering with different imaginary parts of the permittivity ε_r'' is studied in Figure 8. With ε_r'' increasing, the scattering coefficient increases, and BSC of the dielectric rough surface has a slightly increase when ε_r'' increases to some extent. As ε_r'' increases, materials of rough surfaces tend to be a perfectly electric conducting medium. As a result, there is a rise in the scattering coefficient for TE and TM cases when ε_r'' increases, and numerical results approach stability with the increase of ε_r''.

5. CONCLUSIONS

A hybrid FEM/BIE is extended in this paper to study the scattering from dielectric random rough surfaces. Rough surfaces are usually assumed as PEC models in published papers when FEM is applied in the simulation. However, real rough surfaces, such as the ground and the sea, are usually dielectric models. In our hybrid method, conformal integral boundaries are built to truncate the infinite computational region, which can reduce the number of unknowns compared with traditional FEM based on PML or ABC. This hybrid method is versatile and exact in the numerical simulation of dielectric rough surfaces, and can be extended to the problem of an inhomogeneous model easily compared to MoM. Unfortunately, this method needs more time and memory than those of MoM because a mass of unavoidable meshes are generated in FEM domain. In our future work, this topic will be investigated in detail, with focus on scattering from two-dimensional randomly rough surfaces using the FEM/BIE algorithm, the improvement in computational time and memory of the hybrid method, and applications of FEM/BIE for the inhomogeneous models.

ACKNOWLEDGMENT

Project supported by the National Natural Science Foundation for Distinguished Young Scholars of China (Grant No. 61225002), the Specialized Research Fund for the Doctoral Program of Higher Education (Grant No. 20100203110016), and the Fundamental Research Funds for the Central Universities (Grant No. K5051007001).

REFERENCES

1. Ji, W. J. and C. M. Tong, "Bistatic scattering from two-dimensional dielectric ocean rough surface with a PEC object partially embedded by using the G-SMCG method," *Progress In Electromagnetics Research*, Vol. 105, 119–139, 2010.
2. Li, Z.-X., "Bistatic scattering from rough dielectric soil surface with a conducting object with arbitrary closed contour partially buried by using the FBM/SAA method," *Progress In Electromagnetics Research*, Vol. 76, 253–274, 2007.

3. Barka, A. and P. Caudrillier, "Domain decomposition method based on generalized scattering matrix for installed performance of antennas on aircraft," *IEEE Transactions on Antennas and Propagation*, Vol. 55, No. 6, 1833–1842, 2007.
4. Wang, R., L. Guo, J. Li, and X. Liu, "Investigation on transient electromagnetic scattering from a randomly rough surface and the perfect electric conductor target with an arbitrary cross section above it," *Science in China, Series G: Physics, Mechanics and Astronomy*, Vol. 52, 665–675, 2009.
5. Li, J., L. X. Guo, and H. Zeng, "FDTD method investigation on the polarimetric scattering from 2-D rough surface," *Progress In Electromagnetics Research*, Vol. 101, 173–188, 2010.
6. Botha, M. M. and D. B. Davidson, "Rigorous, auxiliary variable-based implementation of a second-order ABC for the vector FEM," *IEEE Transactions on Antennas and Propagation*, Vol. 54, No. 11, 3499–3504, 2006.
7. Zhai, Y. B., X. W. Ping, and T. J. Cui, "Scattering from complex bodies of revolution using a high-order mixed finite element method and locally-conformal perfectly matched layer," *IEEE Transactions on Antennas and Propagation*, Vol. 59, No. 5, 1761–1764, 2011.
8. Liu, P. and Y.-Q. Jin, "Numerical simulation of bistatic scattering from a target at low altitude above rough sea surface under an EM-wave incidence at low grazing angle by using the finite element method," *IEEE Transactions on Antennas and Propagation*, Vol. 52, No. 5, 1205–1210, 2004.
9. Ozgun, O., "Monte Carlo-based characteristic basis finite element method (MC-CBFEM) for numerical analysis of scattering from objects on/above rough sea surfaces," *IEEE Transactions on Geoscience and Remote Sensing*, Vol. 50, No. 3, 769–783, 2012.
10. Chen, Y., S. Yang, S. He, and Z. Nie, "Fast analysis of microstrip antennas over a frequency band using an accurate MoM matrix interpolation technique," *Progress In Electromagnetics Research*, Vol. 109, 301–324, 2010.
11. Alavikia, B. and O. M. Ramahi, "Electromagnetic scattering from cylindrical objects above a conductive surface using a hybrid finiteelement-surface integral equation method," *Journal of the Optical Society of America A: Optics and Image Science, and Vision*, Vol. 28, 2510–2518, 2011.
12. Cui, Z. W., Y. P. Han, C. Y. Li, and W. J. Zhao, "Efficient analysis of scattering from multiple 3-D cavities by means of a FE-BI-DDM method," *Progress In Electromagnetics Research*, Vol. 116, 425–439, 2011.
13. Li, J., L. X. Guo, Q. He, and B. Wei, "Electromagnetic scattering from randomly rough surfaces with hybrid FEM/BIE," *Chinese Physics Letters*, Vol. 28, 104101-1–104101-4, 2011.
14. Ping, X. W., T. J. Cui, and W. B. Lu, "The combination of BCGSTAB with multifrontal algorithm to solve FEBI-MLFMA linear systems arising from inhomogeneous electromagnetic scattering problems," *Progress In Electromagnetics Research*, Vol. 93, 91–105, 2009.
15. Thorsos, E. I., "The validity of the Kirchhoff approximation for rough surface scattering using a Gaussian roughness spectrum," *Journal of the Acoustical Society of America*, Vol. 83, No. 1, 78–92, 1988.
16. Jin, J. M., *The Finite Element Method in Electromagnetics*, John Wiley, New York, 2002.